www.czasopisma.pan.pl PAN www.journals.pan.pl

Metrol. Meas. Syst., Vol. XXIII (2016), No. 1, pp. 133–142.

PAN POLSKA AKADEMIA NAUK

METROLOGY AND MEASUREMENT SYSTEMS

Index 330930, ISSN 0860-8229

www.metrology.pg.gda.pl

M&MS

MEASUREMENT OF SILVER NANOLAYER ABSORPTION BY THE BODY IN AN IN VIVO MODEL OF INFLAMMATORY GASTROINTESTINAL DISEASES

Krzysztof Siczek[1)], Wojciech Pawlak[2)], Hubert Zatorski[3)], Jakub Fichna[3)]

1) Lodz University of Technology, Department of Vehicles and Fundamentals of Machine Design, S. Żeromskiego 116, 90-924, Łódź, Poland (✉ ks670907@p.lodz.pl, +48 42 631 2250)

2) Lodz University of Technology, Institute of Materials Science and Engineering, Stefanowskiego 1/15, 90-924, Łódź, Poland (wojciech.pawlak@p.lodz.pl)

3) Medical University of Lodz, Department of Biochemistry, Mazowiecka 6/8, 92-215, Łódź, Poland (hubert.zatorski@umed.lodz.pl, jakub.fichna@umed.lodz.pl)

Abstract

Layers of silver particles are used in the studies on pathophysiology and treatment of diseases, both in pre-clinical and clinical conditions. Silver layers can be formed using different techniques and on different substrates. Deposition by magnetron sputtering on glass beads was used in this study. Silver absorption by the body was estimated by calculating the difference in thickness of the silver nanolayer deposited on a bead and measured before and after application of the bead in an animal model of gastrointestinal inflammation. Recommendations for the minimal thickness of silver nanolayer deposited on glass beads were worked out for further studies.

Keywords: silver nanolayer, measurement of layer thickness, in vivo animal model.

1. Introduction

The size of *Nanosilver Particles* (NSPs) is generally between 1 and 100 nm in at least one dimension. The increase of surface area-to-volume ratio of such particles accompanied with the decrease of their size can lead to significant changes of their physical, chemical, and biological properties. NSPs are more and more often used in biomedical applications, because of their antibacterial, antifungal, antiviral, and anti-inflammatory activity [1].

Studies on the properties of nanosilver can be carried out using human or animal cells [1], like human peripheral blood mononuclear cells, human alveolar epithelial cell line (A549), human osteoblast cell line, murine and human alveolar macrophage cell line, mouse germline cells, mouse fibroblasts (L929) and rat liver cell line [1]. Research can also be carried out in animal models involving mice and rats [2], or simple model organisms such as *Caenorhabditis Elegans* [3–4].

There are only a few papers describing the impact of silver or nanosilver on the digestive system and the use of this metal for *Gastrointestinal* (GI) diseases. For example, it has been stated in [5] that in physiological conditions nearly 10–20% of the ingested silver metal is absorbed in the GI tract, particularly in the duodenum and small intestine. To examine the GI diseases, mice are often used as the model of choice. The main challenge during the studies of mouse models is introducing a needed dose of silver or nanosilver into the GI tract.

Here, the authors propose the use of small, borosilicate glass beads (about 1 mm in diameter) with layers of silver deposited by magnetron sputtering. The beads coated with silver nanolayer may enable delivering a precise dose of this metal in time and space, depending on the nanolayer diameter and composition (additives). The aim of the study was thus to validate the methods of: 1) silver nanolayer deposition and 2) estimation of silver absorption by the body

Article history: received on Sep. 01, 2015; accepted on Nov. 14, 2015; available online on Feb. 26, 2016; DOI: 1515/mms-2016-0008.

from coated beads in mice being experimentally induced with GI inflammation. The use of silver in GI inflammation has not been so far examined and – if the silver nanolayer deposition proves successful and further studies show its potential anti-inflammatory effect in the inflamed colon – a new therapeutic approach will be ready for clinical trials.

2. Materials and methods

2.1. Theory concerning measurement of nanolayer thickness

One of the frequently used methods of thin film thickness determination is the *X-ray Rreflectivity* (XRR) [6–7]. This is a non-destructive procedure, which enables to determine the film thickness with the angstrom resolution [6]. In the XRR method, the recorded diffraction peaks are correlated with the thickness of the examined layer. The other often used methods are: scanning force microscopy [8], atomic force microscopy [9] and ellipsometry [10].

There is also a limited number of techniques with a sufficient depth resolution to provide composition profiling within a few nanometers from the surface. The most commonly known are: *Transmission Electron Microscopy* (TEM) combined with electron dispersive spectroscopy and/or *Electron Energy Loss Spectroscopy* (EELS) [11]; nuclear techniques such as high-resolution *Rutherford Backscattering Spectrometry* (HR-RBS) [12], *Medium Energy Ion Scattering* (MEIS) [13] or *Elastic Recoil Detection* (ERD) [14]; *Time-of-Flight* (TOF), *Secondary Ion Mass Spectroscopy* (SIMS) [15] and *Angle-Resolved X-ray Photoelectron Spectroscopy* (ARXPS) [12, 16–18].

In addition to the accurate depth resolution and the capability to quantify results, the best technique should be reasonably widespread and routinely available, which limits the use of nuclear analysis techniques. Although SIMS techniques have good nanometer scale profiling capabilities for SiON thin films [19, 20], it was also found that most of the high-k profiles obtained by sputter depth profiling were plagued by ion beam sputtering artefacts [21–23].

Thus, a non-sputtering method like ARXPS, whereby the depth information is based on the depth dependent signal attenuation, may appear a better candidate for thin film composition profiling. However, the latter requires a complex data reconstruction algorithm whose validity and uniqueness of results is still debated [24], and where the potential method limitations even for simple systems such as SiON [25] have been indicated.

Notwithstanding these considerations, ARXPS reconstructed depth profiles have already been applied to many different systems with various successes [18].

In the present study, a Transmission Electron Microscope for cross-section observation to determine the thickness of nanolayers was used [26].

2.2. Theory concerning estimation of silver nanolayer absorption by the body

Estimation of silver nanolayer absorption by the body in the mouse model was accomplished under the assumption that all mice used during the examination can have a very similar absorption. The assumed measure of absorption is the ratio A of the volume V of worn silver to the average time t_{aver} of residence in the mouse body, according to (1):

$$A = \frac{V}{t_{aver}}. \tag{1}$$

The volume V of worn silver is calculated from (2):

$$V = V_1 - V_0 = \frac{4 \cdot \pi}{3 \cdot 8}\left[(d+h)^3 - d^3\right] \approx \frac{\pi}{6} \cdot h \cdot 2 \cdot d^2 = \frac{\pi}{3} h d^2. \tag{2}$$

Metrol. Meas. Syst., Vol. XXIII (2016), No. 1, pp. 133–142.

where: V_0 is the volume of bead with silver nanolayer in the mouse body after treatment; V_1 is the volume of bead with silver nanolayer in the mouse body before treatment; d – the bead diameter with silver nanolayer in the mouse body after treatment; h – the estimated thickness of worn silver nanolayer.

The error of calculation of silver absorption by the body can be estimated from (3):

$$\Delta A \approx \frac{\partial A}{\partial h}\Delta h + \frac{\partial A}{\partial d}\Delta d = \frac{\pi}{3 \cdot t_{aver}}\left(d^2 \Delta h + 2dh\Delta d\right), \tag{3}$$

where: $\Delta h = 30\,\text{nm}$ – the error of silver nanolayer thickness estimation; $\Delta d = 10\,\mu\text{m}$ – the error of diameter measurement.

The average time t_{aver} of residence in the mouse body is assumed to be equal to 12h, according to the procedure of in-mouse treatment, described further.

The estimation of thickness h of worn silver nanolayer is based on the obtained images of bead cross-sections. The layer thickness is placed between two straight border lines: the upper and bottom ones. The positions of such border lines are estimated as follows: in the interfaces between the silver nanolayer and surrounding air and between the silver nanolayer and its substrate there are some discontinuities, visible in the images in the form of white, gray and black areas. Such discontinuities are due to the occurrence of different materials and possible cracks grains. A straight line in the image is divided by pixels into N parts. These parts can be classified into three groups, according to the colour parameter of a pixel crossed by the straight line. Let the number k means the number of group, where $k = 1$ for the white area, $k = 2$ for the grey area and $k = 3$ for the black area. The length of the i-th part, where $i = 1..N$, belonging to the k-th group is designated as l_i^k. The position of border line is assumed to comply with the criterion given by (4):

$$\frac{\sum_{k=2}^{k=3}\sum_{i=1}^{i=N} l_i^k}{\sum_{k=1}^{k=3}\sum_{i=1}^{i=N} l_i^k} \le 0.05\,. \tag{4}$$

This means that both straight border lines should contain at least 95% areas of silver nanolayer. This is obtained numerically.

2.3. Sample preparation

Borosilicate glass beads with the diameter from 850 to 1400 μm were placed in a special holder in the magnetron sputtering unit. The holder enables uniform mixing of glass beads during silver layer deposition. For deposition, a simple magnetron sputtering method using a standard 2" magnetron sputtering gun equipped with a pure silver (4N) target was chosen. The actual weight of glass beads per each deposition was set to about 0.5 g. After reaching the base pressure of $5\text{x}10^{-3}$ Pa in the vacuum chamber, pure argon (5N) was compressed to the working pressure of 0.7 Pa. Deposition of silver layer lasted 360 s with the sputtering power of 270 W. After deposition, the coated beads were divided into the beads used in structural and in vivo examinations. Consequently, SEM observations of the microstructure of the coatings as well as EDS analysis of chemical composition were performed. In order to measure the thickness, modern techniques of *Focused Ion Beam* (FIB) in a stationery unit of ion polisher JEOL-09010CP as well as FIB/SEM system of FEI FIB-Quanta 3D and FEI Tecnai FEG (200 kV) *Transmission Electron Microscope* (TEM) for cross-section observations were used [26]. *Transmission Electron Microscope* Tecnai G2 F20 (200kV) is equipped with: a *Field Emission*

Gun (FEG), high resolution Gatan UltraScan and wide angle SIS Megaview cameras, an HAADF detector intended for the *Scanning-Transmission Technique* (STEM), an EDAX X-ray spectrometer for analysis of the chemical composition. FEI FIB-Quanta 3D is a "dual beam" *Scanning Electron Microscope* (SEM) that is also equipped with a *Focused Ion Beam* (FIB). These SEM functions enable microscopic observations of an examined sample, while the FIB functions enable cutting it. This FEG-SEM-FIB has an Omniprobe for TEM sample preparation. An SDD EDS analyzes elemental chemistry of the sample. In addition, an *Electron Backscattered Diffraction System* (EBSD) collects the crystallography information from the sample. Using these capabilities together enables learning about, or modifying, the sample's three dimensional (3D) structure and chemistry. It also has a plug in STEM and backscatter detectors, as well as environmental SEM capability.

A similar technique was used for the samples after the time of the beads residing in the mouse gastrointestinal system.

2.4. Mouse model of colonic inflammation and treatment with silver-coated glass beads

Male balbC mice weighing 22–25 g were used throughout the study. On Day 0, the animals were randomly divided into three experimental groups (n = 6–8 animals per group): 1) non-inflamed controls; 2) inflamed controls and 3. inflamed mice treated with silver-coated glass beads. Colonic inflammation was induced on Day 0 by *intracolonic* (i.c.) administering *Trinitrobenzenesulfonic Acid* (TNBS), as described previously in [27]. The mice from experimental group #3 were treated with silver-coated glass beads (5 beads/animal, i.c., twice daily) between Day 3 and Day 6. On Day 7, all animals were euthanized and inflammation score was assessed, as described previously in [27]. Briefly, the colon was removed, opened longitudinally, rinsed with *Phosphate Buffered Saline* (PBS), and immediately examined. The macroscopic colonic damage was assessed with an established semi-quantitative scoring system by adding individual scores for ulcer, colonic shortening, wall thickness, and presence of hemorrhage, fecal blood, and diarrhea. For scoring ulcer and colonic shortening the following scale was used: ulcer – 0.5 points for each 0.5 cm; shortening of the colon: 1 point for >15%, 2 points for >25% (based on a mean length of the colon in untreated mice). The wall thickness was measured in mm: a thickness of n mm corresponds to n scoring points. The presence of hemorrhage, fecal blood, or diarrhea increased the score by 1 point for each additional feature.

3. Results

3.1. SEM/EDS mapping

Figure 1 shows the view of one arbitrarily chosen bead after deposition of the Ag layer made using *Secondary Electrons* (SE). In Fig. 2., the surface arrangement of the elements present in the studied system is shown. The chemical composition is shown in Table 1.

Table 1. The chemical composition of the bead from Fig. 2 and Fig. 3 revealed with the EDS method. Carbon and oxygen were removed from analysis due to low sensitivity of EDS methods.

Figure number	ELEMENT	Na	Al	Si	S	Ca	Ti	Zn	Ag
2	ATOMIC %	11.6	1.4	35	4.1	10.4	3.1	2.5	31.9
3	ATOMIC %	13.7	0	41.3	2.4	11.8	0	0	30.8

Metrol. Meas. Syst., Vol. XXIII (2016), No. 1, pp. 133–142.

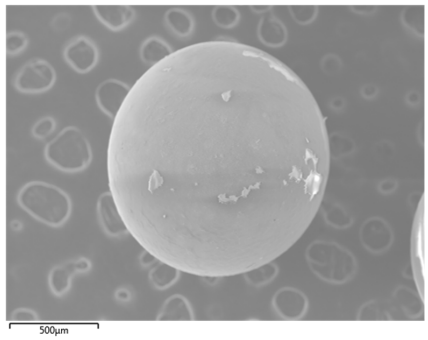

Fig. 1. A bead covered with the pure Ag layer. Defects are clearly seen. Small magnification. Background: a carbon tape for SEM observations.

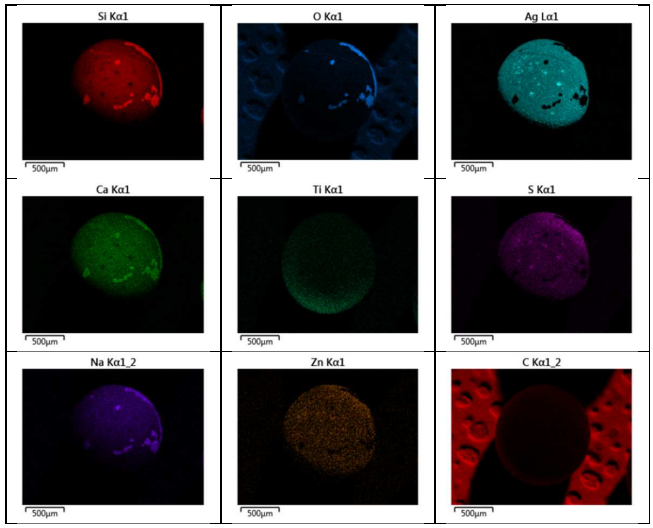

Fig. 2. The EDS mapping results of the deposited Ag layer onto a glass bead.

Figure 3 shows the microstructure of glass beads after application in the mouse gastrointestinal tract. Table 1 shows the chemical composition of in-mouse-treated surface.

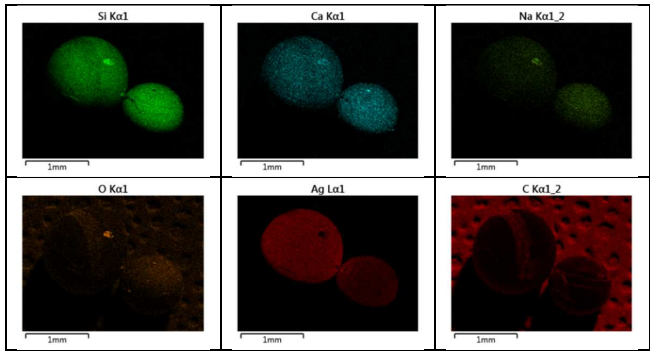

Fig. 3. The EDS mapping results of the deposited Ag layer onto a glass bead after in vivo "dissolution" in the mouse gastrointestinal tract.

3.2. Analysis of thickness with TEM/HAADF technique

In Fig. 4, a STEM Image of the Ag layer before its application in the animal model is presented. The chemical analysis patterns of points 1 and 2 from Fig. 4 have been shown in Fig. 5.

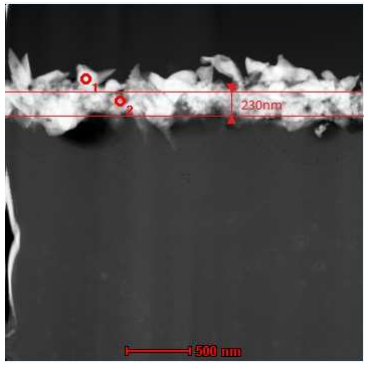

Fig. 4. A STEM Image of the Ag layer. Upper dark area: a carbon layer from the preparation method for TEM; Lower dark area: glass bead material. Points O1 and O2 show the chemical analysis areas.

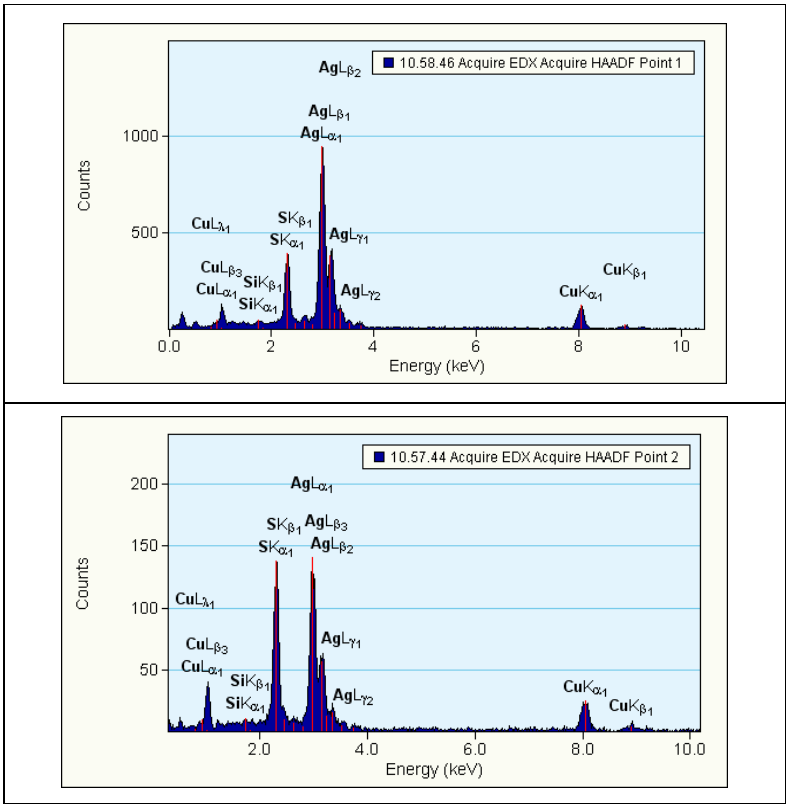

Fig. 5. The chemical analysis patterns of points 1 and 2 from Fig. 4. The interestingly strong signal from sulphur in comparison with the silver one.

Metrol. Meas. Syst., Vol. XXIII (2016), No. 1, pp. 133–142.

From Figs 1 and 2 and Table 1 it is clearly seen that the silver coating is rather thin because the signal of silicon, sodium, calcium and aluminium from the glass substrate is very strong (up to 60% of the sum of signals). Moreover, the silver coating contains sulphur, what is a common phenomenon when silver is stored in the air atmosphere. The maps of element distribution show a discontinuity of the deposited coating. It may suggest a low level of adhesion of the silver layer to the glass bead.

In Fig. 6 a STEM Image of the Ag layer after its application in the animal model is presented. The chemical analysis pattern of point 1 from Fig. 6 has been shown in Fig. 7.

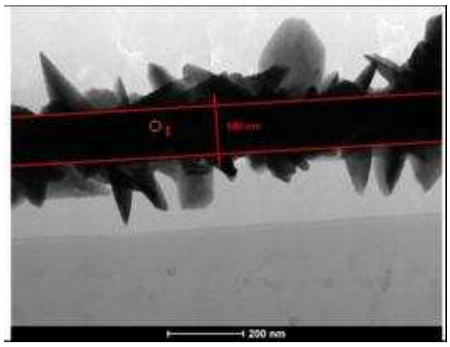

Fig. 6. A STEM Image of the Ag layer. Upper dark area: a carbon layer from the preparation method for TEM; Lower dark area: glass bead material.

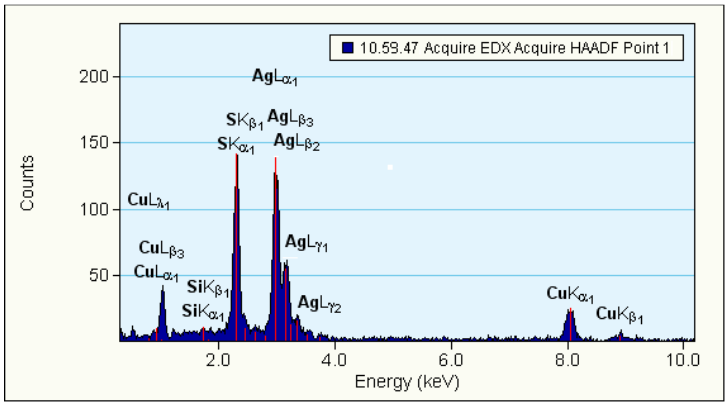

Fig. 7. The chemical analysis pattern of point 1 from Fig. 6. The interestingly strong signal from sulphur in comparison with the silver one.

TEM analysis of cross-section accomplished with the FIB method reveals the real thickness of the silver layer. It was estimated to be about 230 ± 30nm for the deposited coating and about 180 ± 30 nm for the in-mouse treated surface.

3.3. Estimation of silver absorption by the body

The value of silver absorption by the body is obtained using (1) and (2). The sample values, for different bead diameters, are presented in Table 2. The relative error for estimation of silver absorption by the body is relatively high (62%); therefore such estimation can be treated as coarse.

Table 2. The values of silver absorption by the body in the mouse model.

BEAD DIAMETER [μm]	ABSORPTION [μm³/h]	ERROR [μm³/h]	RELATIVE ERROR [%]
850	3151	1964	62
1400	8548	5251	61

3.4. Colonic inflammation in mice reduced by silver-coated glass beads

The i.c. administering TNBS in mice induced severe colonic inflammation, as shown by the increased total macroscopic score, ulceration of the intestinal wall and myeloperoxidase activity, compared with the control animals. The treatment with silver-coated glass beads significantly decreased the macroscopic score (2.12 ± 0.27 vs. 5.62 ± 1.01 for TNBS-alone treated mice, $^{*}p < 0.05$) and clinical parameters of colonic inflammation. The anti-inflammatory effect of the treatment with silver-coated glass beads was confirmed by histopathological analysis of the intestinal tissues.

4. Discussion

The surface of silver nanolayer on the beads excreted from mice was more lustrous than on the beads before introducing them into the mouse gastrointestinal tract. This indirectly indicates interactions between nutritional juice and/or the mouse tissues and the silver layer. The increase of sulphur content in the in-mouse-treated silver nanolayer can be due to food remains in the gastric system.

The estimated minimum thickness of the silver nanolayer that enables to estimate the intensity of interaction between silver and nutritional juices and / or the mouse tissues is 50 nm. To the best of our knowledge, this is the first report that validates this value in conditions applied throughout the study.

5. Conclusions

The minimum thickness of silver nanolayer deposited on glass beads used in the animal models of gastric diseases should be higher than 50 nm. The sulphur content in the in-mouse-treated silver nanolayer can increase due to food remains in the gastric system.

Acknowledgements

The research was supported by the National Science Centre (#UMO-2013/11/B/NZ7/01301 and UMO-2014/13/B/NZ4/01179 to JF) and Medical University of Lodz (503/1-156-04/503-01). Hubert Zatorski is a recipient of Diamentowy Grant from the Ministry of Science and Higher Education in Poland.

References

[1] Ge, L., Li, Q., Wang, M., Ouyang, J., Li, X., Xing, M.M.Q. (2014). Nanosilver particles in medical applications: synthesis, performance, and toxicity. *Int. J. Nanomedicine*, 9, 2399–2407.

[2] Chen, X., Schluesener, H.J. (2008). Nanosilver: a nanoproduct in medical application. *Toxicol Lett.*, 176(1), 1–12.

[3] Hunt, P.R., Keltner, Z., Gao, X., Oldenburg, S.J., Bushana, P., Olejnik, N., Sprando, R.L. (2014). Bioactivity of nanosilver in Caenorhabditis elegans: Effects of size, coat, and shape. *Toxicology Reports*, 1, 923–944.

[4] Walczyńska-Gładysz, M. (2015). *Characterization of biomaterials and nanotechnology products using a model multicellular organism Caenorhabditis elegans.* PhD Thesis, Lodz University of Technology.

[5] Boosalis, M.G., McCall, J.T., Ahrenhalz, D.H., Solem, L.H., McClain, C.J. (1987). Serum and urinary silver levels in thermal injury patients. *Surgery*, 101, 40–43.

[6] Gibaud, A., Hazra, S. (2000). X-ray relectivity and diffuse scaterring. *Current Science*, 78(12), 1467–1477.

[7] Lu, Z.H., McCaffrey, J.P., Brar, B., Wilk, G.D., Wallace, R.M., Feldman, L.C., Tay, S.P. (1997). SiO2 film thickness metrology by x-ray photoelectron spectroscopy. *Appl. Phys. Lett.*, 71, 2764.

[8] Danzebrink, H.U., Koenders, L., Wilkening, G., Yacoot, A., Kunzmannl, H. (2006). Advances in Scanning Force Microscopy for Dimensional Metrology. *CIRP Annals-Manufacturing Technology*, 55, 841–878.

[9] Schaub, A., Slepicka, P., Kasparkova, I., Malinsky, P., Mackova, A., Svorcík, A. (2013). Gold nanolayer and nanocluster coatings induced by heat treatment and evaporation technique. *Nanoscale Research Letters*, 8, 249.

[10] Losurdo, M., Bergmair, M., Bruno, G., Cattelan, D., Cobet, C., de Martino, A., Fleischer, K., Dohcevic-Mitrovic, Z., Esser, N., Galliet, M., Gajic, R., Hemzal, D., Hingerl, K., Humlicek, J., Ossikovski, R., Popovic, Z.V., Saxl, O. (2009). Spectroscopic ellipsometry and polarimetry for materials and systems analysis at the nanometer scale: state-of-the-art, potential, and perspectives. *J. Nanopart. Res.*, 11, 1521–1554.

[11] Halimaoui, A., Henrisey, E., Hernandez, C., Martins, J., Paoli, M., Regache, M., Vallier, L., Bensahel, D., Blanchard, B., Rouchon D., Martin, F. (1998). Tailoring of the Nitrogen Profile in Thin Gate Oxides Using Substrate Nitridation by Nitric Oxide. *MRS Proceedings*, 532, 159.

[12] Kimura, K., Nakajima, K., Conard, T., Vandervorst, W., Bergmaier, A., Dollinger, G. (2010). Analysis of ultra-Thin HfO2/SiON/Si(001): Comparison of three different techniques. *Analytical Sciences*, 26.2, 223–226.

[13] Reading, M.A., van den Berg, J.A., Zalm, P.C., Armour, D.G., Bailey, P., Noakes, T.C.Q., Parisini, A., Conard, T., de Gendt, S. (2010). High resolution medium energy ion scattering analysis for the quantitative depth profiling of ultrathin high-k layers. *Journal of vacuum science & technology B. Microelectronics and nanometer structures: processing, measurement, and phenomena: an official journal of the American Vacuum Society*, 28(1), C1C65-C1C70.

[14] Dollinger, G., Frey, C.M., Bergmaier, A., Faestermann, T. (1998). Depth profile analysis with monolayer resolution using elastic recoil detection. *Europhys. Lett.*, 42, 25.

[15] Brijs, B., *et al.* (2000). Characterization of ultra thin oxynitrides: A general approach. *Nucl. Instrum. Methods Phys. Res.* B, 161, 429.

[16] Brundle, C.R., Conti, G., Mack, P. (2010). XPS and angle resolved XPS, in the semiconductor industry, Characterization and metrology control of ultra-thin films. *J. Electron Spectrosc. Relat. Phenom.*, 178, 433.

[17] Herrera-Gomez, A., *et al.* (2009). Report on the 47th IUVSTA Workshop 'Angle-Resolved XPS: The Current Status and Future Prospects for Angle-resolved XPS of Nano and Subnano Films. *Surf. Interface Anal.* 41, 840.

[18] Conard, T., Vandervorst, W., Bergmaier, A., Kimura, K. (2012). Thin layer composition profiling with angular resolved x-ray photoemission spectroscopy: Factors affecting quantitative results. *Journal of Vacuum Science & Technology A*, 30(3).

[19] Douglas, M.A., Hattangady, S., Eason, K. (2000). Depth Profile Analysis of Ultrathin Silicon Oxynitride Films by TOFSIMS. *J. Electrochem. Soc.* 147, 1893.

[20] van Berkum, J.G.M., Hopstaken, M.J.P., Snijders, J.H.M., Tamminga, Y., Cubaynes, F. (2003). Quantitative depth profiling of SiOxNy layers on Si. *Appl. Surf. Sci.*, 203, 414.

[21] de Witte, H., Conard, T., Vandervorst, W., Gijbels, R. (2003). Ion-bombardment artifact in TOF-SIMS analysis of ZrO2/SiO2/Si stacks. *Appl. Surf. Sci.*, 203, 523.

[22] Conard, T., Vandervorst, W., de Witte, H., van Elshocht, S. (2004). Nitrogen analysis in high-k stack layers: a challenge. *Appl. Surf. Sci.*, 231, 581.

[23] Vandervorst, W., Bennett, J., Huyghebaert, C., Conard, T., Gondran, C., de Witte, H. (2004). On the reliability of SIMS depth profiles through HfO 2-stacks. *Appl. Surf. Sci.*, 231, 569.

[24] Bennett, J., Beebe, M., Sparks, C., Gondran, C., Vandervorst, W. (2004). Sputter rate variations in silicon under high- k dielectric films. *Appl. Surf. Sci.*, 231, 565.

[25] Powell, C.J., Werner, W.S.M., Smekal, W. (2006). Distinguishability of N composition profiles in SiON films on Si by angle-resolved x-ray photoelectron spectroscopy. *Appl. Phys. Lett.*, 89, 172101.

[26] *http://www.imim.pl/labs/205* (Nov. 2015)

[27] Sobczak, M., Mokrowiecka, A., Cygankiewicz, A.I., Zakrzewski, P.K., Salaga, M., Storr, M., Kordek, R., Malecka-Panas, E., Krajewska, W.M., Fichna, J. (2014). Anti-inflammatory and antinociceptive action of an orally available nociceptin receptor agonist SCH 221510 in a mouse model of inflammatory bowel diseases. *J. Pharmacol. Exp. Ther.*, 348, 401–409.